
HILBERT FLATTENING: A LOCALITY-PRESERVING MATRIX UNFOLDING METHOD

A PREPRINT

 **Qingsong Zhao**
Tongji University, China
qingsongzhao@tongji.edu.cn

 **Zhipeng Zhou**
Chinese Academay of Sciences, Beijing, China
zhouzhipeng113@mails.ucas.ac.cn

 **Yi Wang**
Shanghai AI Laboratory, China
wangyi@pjlab.org.cn

 **Yu Qiao**
Shanghai AI Laboratory, China
qiaoyu@pjlab.org.cn

 **Cairong Zhao** 
Tongji University, China
zhaocairong@tongji.edu.cn

January 31, 2023

ABSTRACT

Zigzag flattening (ZF) is commonly utilized as a default option to get the image patches ordering in deep models, *e.g.*, vision transformers (ViTs). Notably, when decomposing multi-scale images, ZF could not maintain the invariance of feature point positions. To this end, we investigate Hilbert flattening (HF) as an alternative for sequence ordering in vision tasks. Specifically, we give the theoretical bounds of HF and ZF in maintaining the spatial locality of the input features, showing the superiority of HF over ZF in matrix unfolding. Moreover, we further prove that such locality-preserving capability of HF is robust against the input scale variance in theory. In the application of HF, we design a Hilbert patch embedding for transformers to empirically demonstrate its scale-invariant locality-preserving in image classification and segmentation. This is also validated in feature down-sampling and feature/image interpolation. Extensive experiments demonstrate that it can yield consistent performance boosts for several popular architectures and applications.

1 Introduction

Flattening is a crucial operation in computer vision, converting a multi-dimensional feature map or image into one dimensional vector. In deep learning, when needing extract semantics from the learned feature maps or tokens, we flatten these high-dimensional inputs into a vector of high-level representation, neglecting localization information.

Though localization descriptions in flattened results are usually oblivious, the specific flatten approaches still contain some of them. Taking the mostly used “zigzag” as an example, most feature points in zigzag flattened vectors are spatially neighboring (1-pixel away) in their original 2D formation, except turning points in zigzag scanning. With the size increase of the feature map for flattening, these 1D distances to the neighboring points of these outcast ones in vector format would be more distorted. In some vision applications, *e.g.*, patch embedding of vision transformer, it would require position compensation techniques (like position encodings) for persevering model performance when using flatten. Generally, a fancy position encoding designs will bring non-trivial performance gains in a negligible cost.

From this perspective, we wonder whether there exists a flatten manner could preserve the theoretically upper-bound of localization information in vector format from matrix one. If so, such a flatten approach whether could bring benefits to current position encoding studies. Further, it may bring research paradigm change as it could just flatten the input signals (with any forms) into a vector for processing, outlining the significance of 1D operators like fully connected layer and depthwise separable convolution.

Inspired by Hilbert fractal theories, we propose a Hilbert Flattening as an alternative for sequence ordering in computer vision. In our investigation, HF has proven to be superior to other methods in maintaining spatial locality, when performing multi-scale transformations of dimensional space in Mathematics Moon et al. [2001]. But, in this paper,

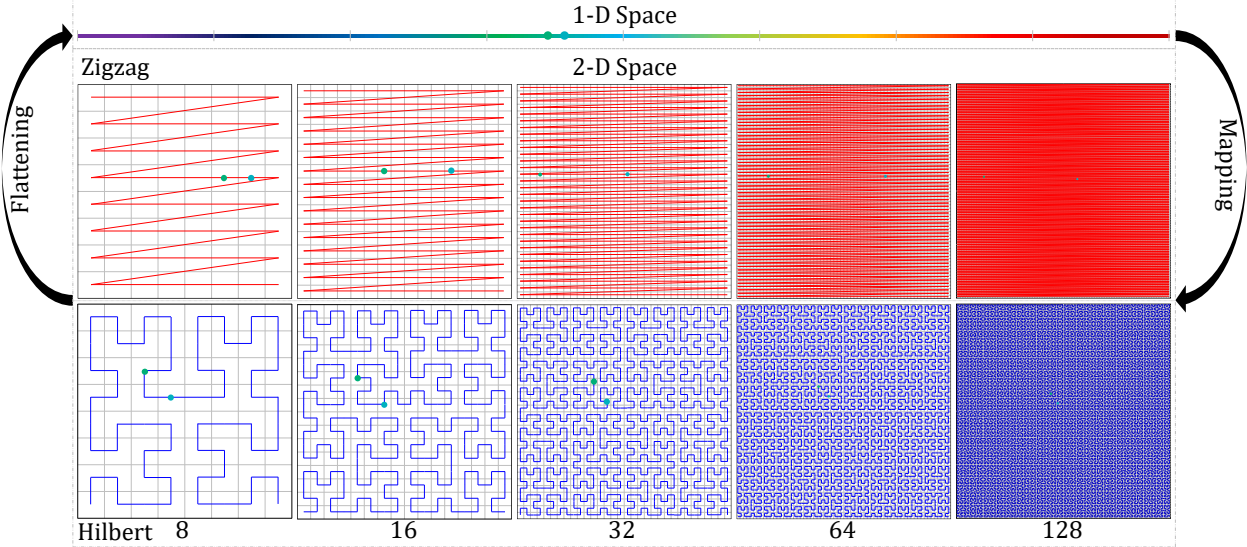


Figure 1: Multi-scale transformation of dimensional space with Zigzag flattening and Hilbert flattening, respectively.

we give a concrete analysis of the theoretical guarantees of HF and ZF in position preserving, and we formulate the nature of the Hilbert fractal in image dimensional transformation and derive its scale robustness accordingly. Further, we validate the practical effectiveness of HF by finding its applications as Hilbert patch embedding, Hilbert feature down-sampling, and Hilbert image interpolation, beyond its theoretical merits. Our contributions can be summarized as follows:

- Through theoretical analysis and experimental supports, we attempt to give one alternative flattening approach named Hilbert flattening in the current vision community. It can preserve much more position information than zigzag and show robustness in dimension scaling.
- We present theoretical evidence that the consecutive parts in sequence by HF are close in the corresponding image. Specifically, we have theoretically estimated the square-to-linear dilation factor of the finite approximation of the Hilbert curve. Meanwhile, The Average Square Distance was proposed to give a quantitative description of the comparison between inverse Hilbert flattening and inverse Zigzag flattening on the probability of points close in 2D being close in a linear sequence. Additionally, we give both theoretical and empirical evidence to demonstrate that HF can maintain feature consistency in multi-scale images.
- We proposed a new patch embedding method based on HF, named Hilbert Patch Embedding (HPE), dedicated to the preservation of local relative position information when flattening the 2D image into a 1D sequence, considering both effectiveness and simplicity. Experiments demonstrate that, without introducing additional hyperparameters, it achieves consistent performance gains in image classification tasks based on multiple network architectures (*e.g.*, ViTs, and Multi-layer Perceptron Networks (MLPs)). In particular, it has better length extrapolation Press et al. [2021] in dense prediction tasks (which is more reliable on the absolute position encoding), *i.e.*, reduces the effect of inconsistent training and prediction token lengths.

2 Related Works

Hilbert Curves. Such prominent works in Mathematics as Jagadish [1990], Gotsman and Lindenbaum [1996], Moon et al. [2001] have evidenced that the locality between objects in multi-dimensional space is preserved in linear space. Inspired by this idea, recent works consisting of Tsinganos et al. [2019], Bappy et al. [2019], Zhang et al. [2021] have been proposed to introduce the Hilbert curves into a computer vision (CV) application. Bappy et al. [2019] noted that the order of the image patches has a significant impact on the performance of the Long-Short Term Memory (LSTM), and if the zigzag flattening was performed in the horizontal direction, the neighboring blocks in the vertical direction are far apart. Eventually, the LSTM may not establish the connection between those patches well. So they utilized the Hilbert curves to arrange image patches before the block sequences were fed into the LSTM. Similarly, to extract better spatial features, FDPT Zhang et al. [2021] also utilized the Hilbert curves to flatten image patches before feeding them into the Gated Recurrent Unit (GRU). By contrast, Tsinganos et al. [2019] employed the Hilbert curves to generate

2D image representations from 1D surface electromyography (sEMG) signals, then the features of the sEMG signals were extracted by the CNN-based backbones. These above methods only apply the Hilbert curve to a CV task without theoretical analysis and empirical proofs.

ViTs and MLPs. Vision Transformer Dosovitskiy et al. [2021] inspires a new paradigm architecture that differs from CNNs by utilizing patch embedding instead of taking images directly as input. Swin Transformer Liu et al. [2021a] proposes shifted windows to solve larger variations of the input image caused by the multi-scale and high resolution. By contrast, MLP-Mixer Tolstikhin et al. [2021] proposed a new architecture that differs from CNNs and Transformers by eliminating the need for convolution and self-attention, and relies only on the repeated implementations of multi-layer perceptron across the spatial or feature channels. Those works above all employed zigzag flattening to expand 2D images or features into 1D patch or pixel sequences. But the ZF would move the initially adjacent image blocks (semantically related patches) away from each other, but HF does not, see Fig. 1 for details. Hence, we explored Hilbert curves whose cluster properties outperform zigzag curves for those ViTs and MLPs based architectures.

3 Hilbert Flattening

Hilbert flattening is built upon Hilbert curve, so we begin this section with an introduction to Hilbert curve, then define Hilbert flattening. After that, we show properties of Hilbert flattening and its applications. The definitions and known theorems used in this paper mainly come from Sagan [2012], please refer to it for more details.

3.1 Definition

Hilbert Curve. We denote \mathcal{I} and \mathcal{Q} as the interval $[0, 1]$ and square $[0, 1] \times [0, 1]$ respectively. The generating process of Hilbert curve is driven by the following:

$$\begin{aligned} \mathcal{H} : t \in [0, 1] &\mapsto \mathcal{H}(t) \in [0, 1] \times [0, 1], \\ t = 0.q_1q_2 \dots, 0 \leq q_j &\leq 3, \\ \mathcal{H}(t) &= \left(\begin{smallmatrix} \mathcal{R}e \\ \mathcal{I}m, \end{smallmatrix} \right) \lim_{n \rightarrow \infty} T_{q_1} T_{q_2} \dots T_{q_n} \mathcal{Q}, \end{aligned} \quad (1)$$

where t is represented in quaternary form. The definition of $\{T_i | 0 \leq i \leq 3\}$ is defined as follows:

$$\begin{aligned} T_i z &= \frac{1}{2} H_i z + h_i, 0 \leq i \leq 3, \\ H_0 z &= \bar{z}i, H_1 z = z, H_2 z = z, H_3 z = -\bar{z}i, \\ h_0 &= 0, h_1 = \frac{i}{2}, h_2 = \frac{1+i}{2}, h_3 = \frac{2+i}{2}, \end{aligned} \quad (2)$$

where we consider complex numbers $z \in \mathbb{C}$ as $(Re(z), Im(z)) \in [0, 1] \times [0, 1]$. The transformations $\{T_i | 0 \leq i \leq 3\}$ defined above corresponds to different geometric deformations. Take transformation T_0 as an example, we first shrink the original \mathcal{Q} towards the original point under the ratio $\frac{1}{2}$, then reflect on the imaginary axis by multiplying with -1 and rotate the square through 90° by multiplying with imaginary number i .

As the order of Hilbert curve increases, the sub-squares shrink into points, which claims that $\mathcal{H}(t)$ is a point in \mathbb{R}^2 . Moreover, for **finite quaternaries** which are end or beginning points of sub-intervals of partition of \mathcal{I} , we have

$$\begin{aligned} \mathcal{H}(0.q_1q_2 \dots q_n) &= \left(\begin{smallmatrix} \mathcal{R}e \\ \mathcal{I}m \end{smallmatrix} \right) \sum_{j=1}^n \frac{1}{2^j} H_{q_0} H_{q_1} H_{q_2} \dots H_{q_{j-1}} h_{q_j}, \\ &= \sum_{j=1}^n \frac{1}{2^j} (-1)^{e_{0j}} \text{sgn}(q_j) \begin{pmatrix} (1-d_j)q_j - 1 \\ 1 - d_j q_j \end{pmatrix} \\ \text{sgn}(x) &= \begin{cases} 1, & \text{if } x > 0, \\ 0, & \text{if } x = 0. \end{cases} \\ e_{kj} &= \#(\text{"k" preceding } q_j) \bmod 2, \\ d_j &= e_{0j} + e_{3j} \bmod 2, \end{aligned} \quad (3)$$

where $\#$ is the counting function and $k \in \{0, 3\}$. We have drawn the image points of finite quaternaries ($3 \leq n \leq 7$) connected by straight lines in Figure 1. We call n -th iteration as the approximation of Hilbert curve of order n . As

shown in Figure 1, note that the order n approximation of Hilbert curve originates in the lower-left sub-square and terminates in the lower-right sub-square. The exit point from each sub-square coincides with the point which goes into the following sub-square.

Hilbert Flattening. With approximation of Hilbert curve of order n , we can define the operation Hilbert Flattening. Consider an image with resolution $n \times n$, the inverse map of approximation of Hilbert curve of order n provides the mechanism of Hilbert Flattening of order n :

$$\mathcal{H}^{-1} : \left(\begin{array}{c} \frac{i}{2^n} + \frac{1}{2^{n+1}} \\ \frac{j}{2^n} + \frac{1}{2^{n+1}} \end{array} \right) \mapsto = 0.q_1 q_2 \cdots q_n, \quad (4)$$

where $\mathcal{H}(0.q_1 q_2 \cdots q_n) = (\frac{i}{2^n} + \frac{1}{2^{n+1}}, \frac{j}{2^n} + \frac{1}{2^{n+1}})^T$. Then the pixel on the image contains point $(\frac{i}{2^n} + \frac{1}{2^{n+1}}, \frac{j}{2^n} + \frac{1}{2^{n+1}})^T$ will be assigned the value $0.q_1 q_2 \cdots q_n$. All the pixels on the images will be ordered by theirs values, which in fact give the definition of Hilbert Flattening. The relative position information of the pixels can be preserved under the Hilbert Flattening. We explore it in the following.

3.2 Properties

Compared with the commonly used zigzag, Hilbert flatten owns nice properties in preserving as much locality as possible when flattening an multi-dimensional feature map into an 1D vector. Also, it has another merit that the locality preservation in Hilbert flatten holds steady when the target feature maps are scaling up or down.

3.2.1 Position Information Preservation

Given two points $t_1, t_2 \in [0, 1]$, the quaternary form are represented as $t^1 = 0.q_1^1 q_2^1 \cdots$ and $t^2 = 0.q_1^2 q_2^2 \cdots$ when these two points are close. It means that for an large integer j such that $q_k^1 = q_k^2, \forall 1 \leq k \leq j$. By applying the formula in Equation 3, we obtain the distance between points of $\mathcal{H}(t^1), \mathcal{H}(t^2)$ as follows:

$$|\mathcal{H}(t^1) - \mathcal{H}(t^2)|^2 \leq \sum_{k=j+1} \frac{8}{2^k} \leq \frac{8}{2^j}. \quad (5)$$

The dilation bound of Hilbert curve is shown in Theorem 1,

Theorem 1 *The square-to-linear dilation factor of the Peano-Hilbert curve is equal to 6 Bauman [2006], which means that the maximum value of $\frac{|\mathcal{H}(t^1) - \mathcal{H}(t^2)|^2}{|t^1 - t^2|}$ ≤ 6 .*

Table 1: The percentage of points with $ASD^{\frac{1}{2}}$ smaller than given $ASD^{\frac{1}{2}}$ threshold. Indexing pixel points within the same 2D neighborhood, the larger the percentage indicates the better position information preservation.

$ASD^{\frac{1}{2}}$ threshold	1.4000e-2	1.3778e-2	1.3556e-2	1.3333e-2	1.3111e-2	1.2889e-2	1.2667e-2	1.2444e-2	1.2222e-2	1.2000e-2
ZF	100.00%	96.97%	96.97%	3.13%	3.13%	3.13%	3.08%	3.03%	3.03%	0.00%
HF	80.57%	80.57%	80.57%	80.57%	80.57%	79.54%	78.76%	78.76%	78.76%	76.71%

The HF operation can obtain an sequence ordering of the image/feature map which guarantee that consecutive parts in sequence are close in original image. Now we study the ZF operation on image with size of $H \times W$. For convenience, we can assume that both H and W equal to 2^n . Given a real number $t \in [0, 1]$ which can be represented in quaternary form with finite length: $t = 0.q_1 q_2 \cdots q_n$, the ZF is defined by \mathcal{Z}^{-1} as follows:

$$\mathcal{Z} : 0.q_1 q_2 \cdots q_n \mapsto \left(\begin{array}{c} \left(\sum_{k=1}^n q_k 4^{n-k} \% 2^n \right) * \frac{1}{2^n} + \frac{1}{2^{n+1}} \\ \left\lfloor \frac{\sum_{k=1}^n q_k 4^{n-k}}{2^n} \right\rfloor * \frac{1}{2^n} + \frac{1}{2^{n+1}} \end{array} \right) \quad (6)$$

$$\mathcal{Z}^{-1} : \left[\frac{i}{2^n}, \frac{j}{2^n} \right] \mapsto 0.q_1 q_2 \cdots q_n = \mathcal{Z}^{-1} \left(\left[\frac{i}{2^n}, \frac{j}{2^n} \right] \right), \quad (7)$$

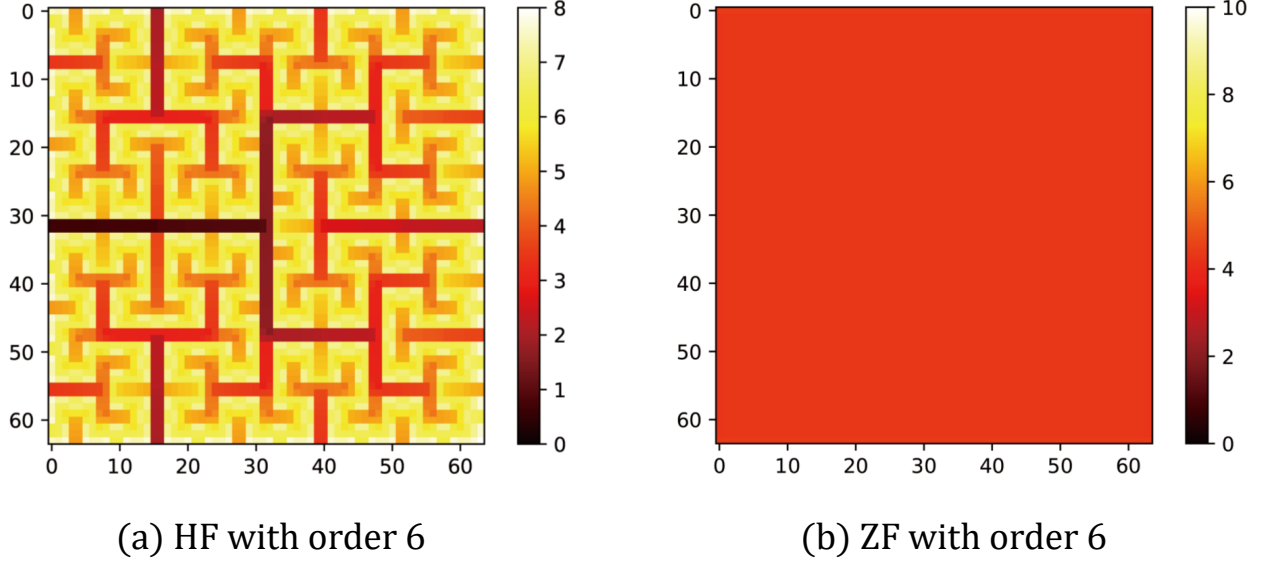


Figure 2: The heatmap of $-\log \text{ASD}^{\frac{1}{2}}$, the brightness of the pixels indicates the 2D position information preservation. The closer the pixels are to white, the better.

where $0 \leq i, j \leq 2^n - 1$. Let $t^1 = 0.\underbrace{00 \cdots 0}_{\frac{n}{2}} \underbrace{33 \cdots 3}_{\frac{n}{2}}$ and $t^2 = 0.\underbrace{00 \cdots 0}_{\frac{n}{2}} \underbrace{100 \cdots 0}_{\frac{n}{2}}$, which are consecutive points in the interval $[0, 1]$ with distance $\frac{1}{4^n}$. Then we have $|\frac{\mathcal{Z}(t^1) - \mathcal{Z}(t^2)|^2}{\frac{1}{4^n}} = \frac{(1 - \frac{1}{2^n})^2 + \frac{1}{4^n}}{\frac{1}{4^n}} = 4^n - 2^{n+1} + 2$. Then we get Remark 1 (our proposed Remark 1 has been utilized in the point cloud classification and segmentation tasks Chen et al. [2022]).

Remark 1 *The square-to-linear dilation factor of the ZF curve is ∞ . ($\lim_{n \rightarrow \infty} 4^n - 2^{n+1} + 2 = \infty$).*

We draw the conclusion ZF operation obtain a sequence ordering of the image/feature map where consecutive points are distant in original image. Now we explore how much HF/ZF can preserve the original 2D structure. For each pixel p at position (i, j) , we collect the neighbors which are K steps away from p . In order to measure the extent of 2D position information preservation, we define the Average Square Distance (ASD) of those pixels respect to p as follows:

$$\text{ASD}(p) = \frac{\sum_{k=i-K}^{i+k} \sum_{l=j-K}^{j+K} (\mathcal{F}^{-1}(p_{kl}) - \mathcal{F}^{-1}(p))^2}{\#(K \text{ step neighbors})}. \quad (8)$$

As shown in Figure 2, most points have an uniform high ASD value under ZF mechanism, while over a certain percentage of points in HF have a small ASD value. Moreover, we give the quantitative comparison between ZF and HF in Table 3.2.1(order 6) on percentage of points whose $\text{ASD}^{\frac{1}{2}}$ is smaller than a given threshold. This shows that HF has an advantage in the preservation of original relative position information over ZF.

3.2.2 Scale Robustness

Take $\Omega = \mathbb{Z}_{2^n} \times \mathbb{Z}_{2^n}$ to be a two-dimensional $2^n \times 2^n$ grid, given an RGB image as an mapping $\Omega \rightarrow \mathbb{R}^3$. As proposed by Bronstein et al. [2021], the convolutional layers of CNNs are shift-equivariant. The general equivariant is defined as follows,

Definition 1 *A function $f : \mathcal{X}(\Omega) \rightarrow \mathcal{X}(\Omega)$ is \mathcal{G} -equivariant if $f(\rho(g)x) = \rho(g)f(x)$ for all $g \in \mathcal{G}$, i.e., group action on the input affects the output in the same way, where $\mathcal{X}(\Omega)$ denotes all signals on domain Ω .*

Definition 2 *A function $f : \mathcal{X}(\Omega) \rightarrow \mathcal{X}(\Omega)$ is \mathcal{G} -robust if $f(\rho(g)x) \approx \rho(g)f(x)$ for all $g \in \mathcal{G}$, i.e., group action on the input affects the output in the same way, where $\mathcal{X}(\Omega)$ denotes all signals on domain Ω .*

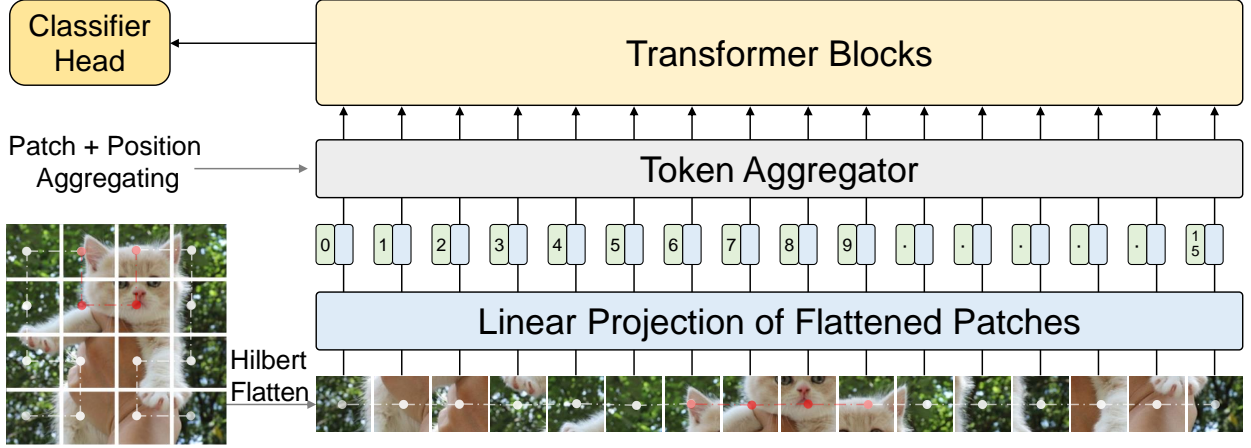


Figure 3: Hilbert patch embedding (HPE). The proposed HPE consists of two critical modules, i.e., Hilbert Patch Flattening (HPF) and Token Aggregator (TA). The HPF would not move the initially adjacent image blocks (semantically related patches) away from each other, e.g., the head of cat (red dotted line) remained clustered together after slicing, and the position of it on the sequence would not change. More detailed introductions turn to Section 3.3.1.

Consider the n -th order and $(n+1)$ -th order approximation of Hilbert curve mapping:

$$\begin{aligned}
 0.q_1q_2 \cdots q_n &\mapsto \sum_{j=1}^n \frac{1}{2^j} (-1)^{e_{0j}} \operatorname{sgn}(q_j) \left(\frac{(1-d_j)q_j - 1}{1 - d_j q_j} \right) \\
 0.q_1q_2 \cdots q_n q_{n+1} &\mapsto \sum_{j=1}^{n+1} \frac{1}{2^j} (-1)^{e_{0j}} \operatorname{sgn}(q_j) \left(\frac{(1-d_j)q_j - 1}{1 - d_j q_j} \right).
 \end{aligned} \tag{9}$$

Geometrically, the above operation just divides the n -th order approximation Hilbert curve uniformly between every pair of end points into three parts, then moves the second part away from the original curve with distance $\frac{1}{2^{n+1}}$. Finally, it connects the moving part with the end points of the second part. (See Figure 1 with $n=3$ and $n=4$). Given an image I with size $2^{n+1} \times 2^{n+1}$, we utilize the $n+1$ -th order HF to flatten it. We denote the image/feature after flattening as $\mathcal{H}_{n+1}(I)$. On the other hand, we scale down the image I into image $I_{\frac{1}{2}}$ with size $2^n \times 2^n$. We denote the image/feature after n -th order HF as $\mathcal{H}_n(I_{\frac{1}{2}})$. Commonly, adjacent pixels usually contain similar information with high probability. $\mathcal{H}_n(I_{\frac{1}{2}})$ and $\mathcal{H}_{n+1}(I)$ satisfy the following condition:

$$(\mathcal{H}_{n+1}(I))_{\frac{1}{2}} \approx \mathcal{H}_n(I_{\frac{1}{2}}), \tag{10}$$

where $\frac{1}{2}$ means that downsampling the image with ratio $\frac{1}{2}$. Consider the scale operation group $\mathcal{S} = \{2^{-m} | m \in \mathbb{Z}\}$, we have

$$(\mathcal{H}_{n+m}(I))_{2^{-m}} \approx \mathcal{H}_n(I_{2^{-m}}). \tag{11}$$

In conclusion, as n approach a sufficiently large number (infinity), we get the Hilbert curve mapping is \mathcal{S} -robust.

3.3 Applications

With the above analysis, we suppose that Hilbert Flattening can be applied to computer vision tasks. For example, we propose a new patch embedding approach based on the position information preservation of HF for the vision transformer models. We introduce a Hilbert sampling methods for the commonly used feature down-up sampling operation in neural network structures based on the scale robustness of HF. The proposed Hilbert sampling also can be utilized in traditional digital image processing tasks e.g., image interpolation.

3.3.1 Hilbert Patch Embedding

Tokens extracted from image patches in transformers are ordered in zigzag by default. We employ HF to process this token order as in Fig. 3. We introduce a new patch embedding method for the Transformer models named Hilbert

patch embedding. As shown in Fig. 3, the Hilbert patch flattening and token aggregator modules collaborate with each other for the next self-attention layers to complete the encoding of patch and position. Different from RNN and CNN, the position encoding is prominent for the Transformer model because the self-attention module only calculates the similarity between the tokens. Two similar tokens may be far apart, but the distance information between these tokens is vital for some computer vision tasks (e.g. object localization). Generally, existing position encoding methods either use relatively simple and direct absolute encoding, or the absolute encoding crucial for detection and localization tasks. Absolute encoding is more sensitive to both the size of the input image and the data inductive bias (e.g. object is always in the center) than relative position coding. From this perspective, we suppose that Hilbert Flatten can alleviate the scale transformation problem in the existing absolute encoding methods.

The Hilbert patch flattening is an unfolding operation for image patches, unlike the orthodox “zigzag” unfolding (e.g., `torch.flatten(·)`), which requires image patches to be flattened in the order of the Hilbert fractal as shown in Fig. 3. The positions between two adjacent tokens in an image are always close to each other Dai et al. [2021], Yuan et al. [2021], which is a widely used assumption in computer vision (aka locality). As introduced in Remark 1, the “zigzag” unfolding will make the adjacent patches to be far away from each other, while HF not. After HPF, it is guaranteed that similar tokens will be close in the flattened one-dimensional sequence. This is necessary for our token aggregator module to work.

For the self-attention to take advantage of this inductive bias (e.g. locality). We introduce a generic token aggregator, which elegantly enhance the similarity between two adjacent tokens. Specifically, for one input sequence, e.g., the embedding of image patches $\mathcal{X} = \{x_1, x_2, \dots, x_n\}$, where $x_i \in \mathbb{R}^D$, n means the number of patches. The output matrix \mathcal{X}' of TA equals to $\{x'_1, x'_2, \dots, x'_n\}$, Each output element x'_i is computed by the Eq. 12 below.

$$x'_i = \mathcal{F}(x_i, k)U_j, \quad (12)$$

where $j \in \{1, 2, \dots, D\}$, $U \in \mathbb{R}^{D \times k}$ is a learnable parameter matrix to integrate n embedded tokens, \mathcal{F} is a function (the output of it $\in \mathbb{R}^{n \times k}$) feeding it x_i that returns a neighborhood of x_i with a radius size k . Therefor, we obtain the aggregated embedding of image patches $x'_i \in \mathbb{R}^D$ and put them into the next self-attention blocks.

3.3.2 Hilbert Feature Sampling

In the feature learning of deep models, it is inevitable to perform up- and down-sampling operations on the feature maps, e.g., super-resolution. Common down-sampling operations include pooling, convolution with step size larger than or equal to 2, etc. Down-sampling operations inevitably lead to information loss, hence a good down-sampling method is required to preserve as much consistent information of the original feature map as possible, in which the consistency is location information or local/global induction bias. From this perspective, we introduce the Hilbert feature down-sampling approach for the feature extraction based on the scale robustness of Hilbert in dimensional transformation. Specifically, unlike traditional “Zigzag” based sampling, we discard or select features or pixels along the Hilbert index to ensure that the selected feature map has a better multi-scale consistency (turn to Appendix B for details).

4 Experiments

We implement the mentioned applications in Sec. 3.3 and validate them in several mainstream benchmarks with popular model architectures and settings. Specifically, we verify the effectiveness of our proposed HF in Hilbert patch embedding (Sec. 4.1) and Hilbert feature sampling (Sec. 4.3). What’s more, we compare the differences between the Hilbert Flattening and Zigzag Flattening methods using the same metrics, e.g., image scaling (Sec. C.1) and dynamic time warping distance (Sec. C.2). More experimental settings, results, and visualizations can be found in the Appendix.

Experimental Setup. We utilized the same model architectures in all baseline settings to compare the performance for fairness. With limited computational resources, we are not motivated by practice-based CV tasks, so we are not good at utilizing the training tricks. Notably, we only change the flattening method in any experiments. Other settings including software and hardware are strictly consistent.

4.1 Hilbert Patch Embedding

As shown in Fig.3, the proposed HPE utilizes the Hilbert flattening strategy and a token aggregator module for better image patch embedding. We employ ViTs and Swin as the backbone of image classification on the ImageNet Deng et al. [2009]. We conduct all experiments by utilizing the same comparison protocols and data augmentation as Radosavovic et al. [2020], Touvron et al. [2021]. The results are reported in Table 2. For ViTs with different scales (e.g., ViT-T, ViT-S, ViT-B, and ViT-L), our HPE can improve them by 0.53%, 0.31%, 0.45%, and 0.45% (Top1 Acc) over their

Table 2: Recognition accuracy of different patch embedding methods on ImageNet with multiple models. \dagger , and \ddagger denote the results reported in Dosovitskiy et al. [2021], and Chen et al. [2021] respectively. * means that some parameters are reduced.

Models	Methods	#Param (M)	Top-1 (%)	Top-5 (%)
ViT-S/16	Original	22.1	78.10 \dagger	-
	Original	86	79.80 \dagger	-
	Original	304	81.10 \dagger	-
	Original	22.1	79.90 \ddagger	-
	Original	21.5	80.70 \ddagger	-
	Original	28.3	81.30 \ddagger	-
	Original	28.1	82.10 \ddagger	95.80
ViT-T/16	Original	5.7	70.38	88.75
	Original	22	80.10	95.19
	Original	86	82.02	95.78
	Original	304	82.98	96.17
	Original	28.1	82.08	95.63
ViT-S/14	HPE	5.7*	70.91	89.22
	HPE	22*	80.41	95.33
	HPE	86*	82.47	96.00
	HPE	304*	83.43	96.44
	HPE	28.1*	82.34	95.85

original methods, respectively. Those improvements are clear and consistent regardless of model size, demonstrating the advantages of the proposed HPE over the original patch embedding. Also, We show that our HPE can bring gains (0.24%) to the Swin model which applies both relative and absolute position encoding methods. One can note that the image classification task is relatively reliable in relative position coding.

Ablation Study. To verify the effectiveness of the proposed two modules in HPE separately, we carry out experiments of image classification both on ImageNet and CIFAR-10 Krizhevsky et al. [2014]. As shown in Table 3, both HPF and TA could achieve non-negligible improvements (i.e., HPF gets 0.17% on ImageNet and 2.47% on CIFAR-10, TA gets 0.12% on ImageNet and 1.40% on CIFAR-10) over the original patch embedding. Moreover, HPF and TA are orthogonal on ImageNet. The combination of them results in the better performance than either one of them.

Table 3: Ablation study. The effect of Hilbert patch embedding and token aggregator on the recognition accuracy for the ViT-B/16 and ViT-T/2 on ImageNet and CIFAR-10 respectively.

Methods	Dataset	HPF	TA	Top-1%	Top-5%
ViT-B/16	ImageNet	-	-	82.02	95.78
ViT-B/16	ImageNet	✓	-	82.19	95.82
ViT-B/16	ImageNet	-	✓	82.14	95.81
ViT-B/16	ImageNet	✓	✓	82.47	96.00
ViT-T/2	CIFAR-10	-	-	83.85	99.00
ViT-T/2	CIFAR-10	-	✓	85.25	99.08
ViT-T/2	CIFAR-10	✓	-	86.32	99.15
ViT-T/2	CIFAR-10	✓	✓	85.71	99.10

Table 4: Finetune recognition accuracy of different patch embedding methods on ImageNet with the ViT-S/14 and ViT-B/16 model. W/o finetune means taking the original model trained with image size 224 directly and test it with 384 inputs.

Models	Methods	Train	Test	Val.	Top-1%	Finetune	W/o Finetune	
		Res.	Res.	Res.	224 ²		Top-1%	W/ 2D Interp.
ViT-S/14	Original	224 ²	336 ²		80.10	81.99	69.89	80.50
ViT-S/14	HPE	224 ²	336 ²		80.41	82.91	78.61	80.89
ViT-B/16	Original	224 ²	384 ²		81.88	83.37	66.03	81.51
ViT-B/16	HPE	224 ²	384 ²		82.13	83.70	69.69	81.67

Specifically, the best score on cifar10 was achieved using only HPF, which indicates that Transformer models have overfitting problems on small datasets (training from scratch).

To compare the transfer ability of the models at different input image scales, We chose pre-trained models trained by Hilbert patch embedding and original patch embedding, respectively. And the fine-tuning performance and the position encoding interpolation-based performance were tested separately. As reported in Table 4, the experimental results show that our HPE has better multi-scale transfer capability. Also, without fine-tuning, only using 1D position encoding interpolation our method achieves an absolute lead (i.e., 8.72% on ViT-S and 3.66% on ViT-B).

To check that our method has better positional encoding capability, we visualize the similarity of position embeddings as shown in Fig. 4. We can see that the absolute position encoding learned utilizing our HPE method is more accurate, which is one of the reasons why our method can bring classification performance improvement on ImageNet. Here, we plot the similarity of position embeddings of them after linear interpolation (the two figures on the right), and we can see that compared to the original patch embedding method, Hilbert flattening retains most of the position information.

4.2 Semantic Segmentation

Our dense prediction (i.e., semantic segmentation) experiments are conducted on ADE20k data set, as reported in Table 6. We adopt the popular and Upernet framework (base on mmseg Contributors [2020]) for a fair comparison. We simply apply the settings of Swin Transformer and train the models for 80k iterations. The drop path rates are set to 0.15/0.35 for small/base variants with Upernet respectively. As shown in Table 6, we can see that the performance impact of

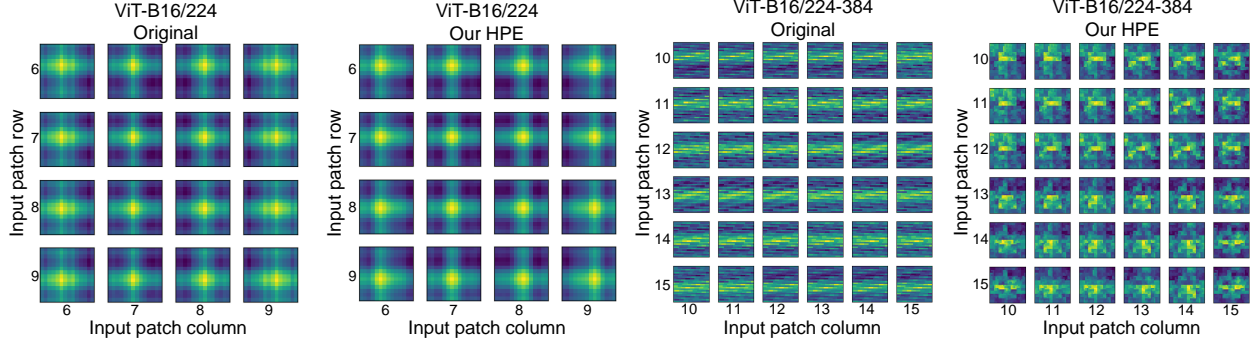


Figure 4: Similarity of position embeddings of ViT-B16 for different patch embedding approaches. The brightness of a pixel indicates the cosine similarity between the position embedding of one patch with the indicated row and column and the other patches. For more clarity, we intercepted the middle position (4×4) of all patches (14×14) for visualization. The two figures on the right are obtained by linear interpolation of the original position embedding. Same as the left figures, we extract the middle position (6×6) of all patches (24×24) for visualization. Turn to the Appendix for more details.

Table 5: Recognition accuracy of different feature sampling methods on CIFAR-10. “HF” indicates that sampling of image patches along the Hilbert flattening index. “ZF” means using the “Zigzag” flattening index. “Overlap” indicates that there is an overlap of sampling points.

Models	Methods	Overlap	Top-1%	Top-5%
Mixer-B/4	ZF	-	79.73	98.34
Mixer-B/4	HF	-	80.59	98.55
Mixer-B/4	ZF	✓	80.48	98.32
Mixer-B/4	HF	✓	81.68	98.57
Mixer-B/8	ZF	-	83.58	98.71
Mixer-B/8	HF	-	84.52	98.83
FPN-MLP	ZF	-	81.42	99.18
FPN-MLP	HF	-	85.71	99.58

position encoding on segmentation is non-trivial. Compared with the original ViT models, our HPE method yields stable gains (0.71% mIoU on ViT-S and 0.86% mIoU on ViT-B). we also plot the learning process of position encoding with model training for our PHE (right) and original (left) patch embedding methods, as shown in Appendix Fig. 11. Those further suggest that our HPE has better multi-scale adaptability.

4.3 Feature Sampling

To prove that better feature sampling can enhance the stability of multi-scale representations, an image pyramid structure based MLPs architecture was employed, turn to Appendix Fig. 7 and Appendix Table 7 for details. We conduct experiments on CIFAR-10, with the commonly used protocols and the data augmentation Lee et al. [2015]. Table 4.1 presents the results of different feature sampling methods. The HF based method can outperform the baseline

Table 6: Semantic segmentation with Upernet 80K Xiao et al. [2018] framework on ADE20K Zhou et al. [2017]. Backbones are taken from our HPE and the original ViT pre-trained on ImageNet, respectively. “Z-Linear” means that down-up sampling the position embedding uses Linear interpolation methods along the Zigzag index. †denotes the results reported in Li et al. [2022] with Upernet 160K. The FLOPs are measured at resolution 512×512 , ‡means the input image size is 512×2048 . * denotes without adding deconvolution.

Backbones	Methods	#Param.(M)	Upernet 80K		
			FLOPs(G)	mIoU(%)	mAcc(%)
ResNet-50Chen et al. [2021]	-	67	951‡	42.05†	-
DeiT-B*Chen et al. [2021]	Original	121	2772‡	44.09†	-
Swin-TLiu et al. [2021b]	Original	60	945‡	44.50†	-
Swin-S3-TChen et al. [2021]	Original	60	954‡	44.87†	-
Focal-TYang et al. [2021]	Original	62	998‡	45.80†	-
Twins-SChu et al. [2021]	Original	54	901‡	46.20†	-
ViT-S/14-336	Original	58	326	44.05	55.02
ViT-S/14-336	HPE	58	326	44.76	56.22
ViT-S/14-336	Z-Linear	58	326	42.22	53.22
ViT-B/16-384	Original	144	395	45.48	57.15
ViT-B/16-384	HPE	144	395	46.34	57.54
ViT-B/16-384	Z-Linear	144	395	44.28	55.80

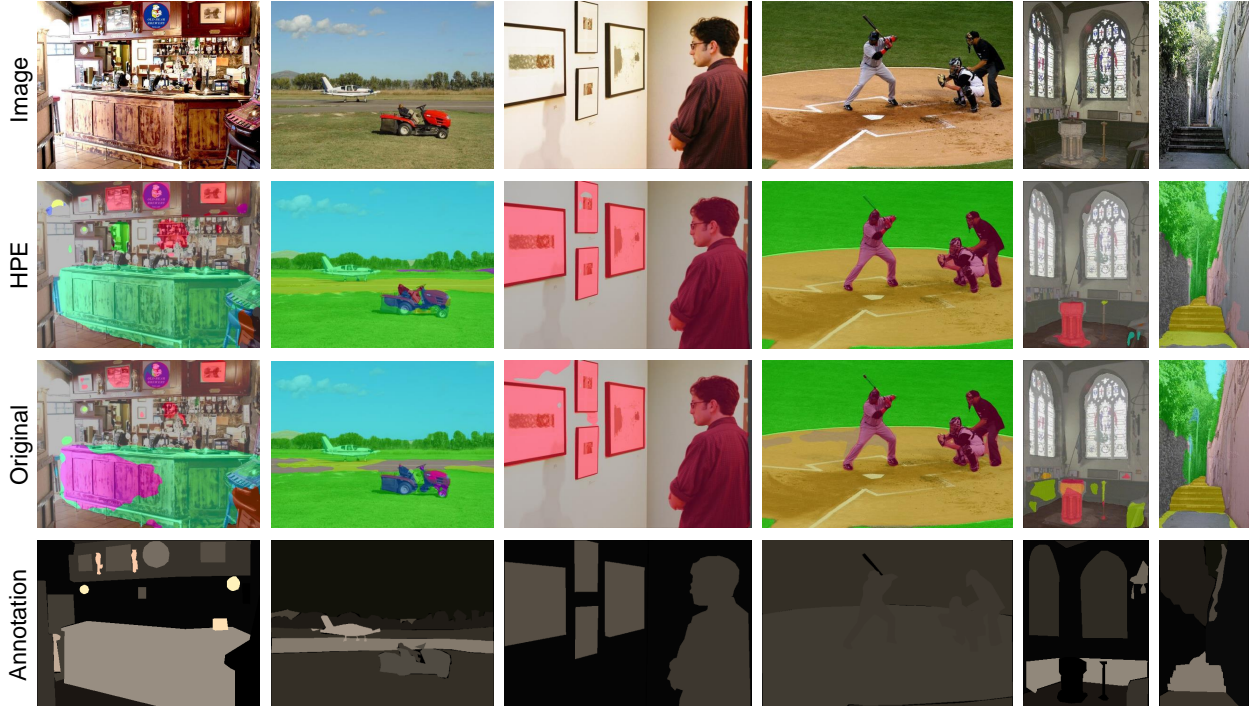


Figure 5: Qualitative results of semantic segmentation on ADE20K Zhou et al. [2017]

of ZF by obvious margins (4.29%). We suppose that compared to ZF, HF can provide stronger stability of multi-scale representations for the model. We also conduct the experiments for the MLPs model (i.e., MLP-Mixer) with different patch flattening approaches (aka embedded patches sampling). As shown in Table 4.1, The results show that the

proposed HF based sampling is effective in MLP-Mixer and also achieves significant improvement based on the Zigzag flattening method. Notably, when we utilize the overlapping strategy, the gap is widened.

5 Conclusion

In this paper, we propose a flattening alternative named Hilbert Flattening. Compared with “zigzag”, HF can well preserve locality in the original 2D form and is robust to scale changes. For the merits of HF, we theoretically evaluate the square-to-linear dilation factor of the finite approximation of Hilbert curve, and propose the Average Square Distance to compare inverse HF with ZF. All these advantages are supported by theoretical analysis and experimental results. Based on the above theorise, we proposed Hilbert patch embedding and Hilbert feature sampling methods for the ViTs and other networks. The code will be released upon acceptance.

References

Bongki Moon, H. V. Jagadish, Christos Faloutsos, and Joel H. Saltz. Analysis of the clustering properties of the hilbert space-filling curve. *IEEE Trans. Knowl. Data Eng.*, 13(1):124–141, 2001.

Ofir Press, Noah A Smith, and Mike Lewis. Train short, test long: Attention with linear biases enables input length extrapolation. *arXiv preprint arXiv:2108.12409*, 2021.

H. V. Jagadish. Linear clustering of objects with multiple attributes. In *Proceedings of the 1990 ACM SIGMOD International Conference on Management of Data, Atlantic City, NJ, USA*, pages 332–342. ACM Press, 1990.

Craig Gotsman and Michael Lindenbaum. On the metric properties of discrete space-filling curves. *IEEE Trans. Image Process.*, 5(5):794–797, 1996.

Panagiotis Tsinganos, Bruno Cornelis, Jan Cornelis, Bart Jansen, and Athanassios Skodras. A hilbert curve based representation of semg signals for gesture recognition. In *International Conference on Systems, Signals and Image Processing, IWSSIP 2019, Osijek, Croatia, June 5-7, 2019*, pages 201–206. IEEE, 2019.

Jawadul H. Bappy, Cody Simons, Lakshmanan Nataraj, B. S. Manjunath, and Amit K. Roy-Chowdhury. Hybrid LSTM and encoder-decoder architecture for detection of image forgeries. *IEEE Trans. Image Process.*, 28(7):3286–3300, 2019.

Xueqi Zhang, Shuo Wang, Chenyu Liu, Min Zhang, Xiaohan Liu, and Haiyong Xie. Thinking in patch: Towards generalizable forgery detection with patch transformation. In *PRICAI 2021: Trends in Artificial Intelligence - 18th Pacific Rim International Conference on Artificial Intelligence*, volume 13033, pages 337–352, 2021.

Alexey Dosovitskiy, Lucas Beyer, Alexander Kolesnikov, Dirk Weissenborn, Xiaohua Zhai, Thomas Unterthiner, Mostafa Dehghani, Matthias Minderer, Georg Heigold, Sylvain Gelly, Jakob Uszkoreit, and Neil Houlsby. An image is worth 16x16 words: Transformers for image recognition at scale. In *9th International Conference on Learning Representations, ICLR 2021, Virtual Event, Austria*, 2021.

Ze Liu, Yutong Lin, Yue Cao, Han Hu, Yixuan Wei, Zheng Zhang, Stephen Lin, and Baining Guo. Swin transformer: Hierarchical vision transformer using shifted windows. In *ICCV*, 2021a.

Ilya O. Tolstikhin, Neil Houlsby, Alexander Kolesnikov, Lucas Beyer, Xiaohua Zhai, Thomas Unterthiner, Jessica Yung, Andreas Steiner, Daniel Keysers, Jakob Uszkoreit, Mario Lucic, and Alexey Dosovitskiy. Mlp-mixer: An all-mlp architecture for vision. *CoRR*, abs/2105.01601, 2021.

Hans Sagan. *Space-filling curves*. Springer Science & Business Media, 2012.

Konstantin Bauman. The dilation factor of the peano-hilbert curve. *Mathematical Notes*, 80:609–620, 11 2006.

Wanli Chen, Xinge Zhu, Guojin Chen, and Bei Yu. Efficient point cloud analysis using hilbert curve. In *Computer Vision–ECCV 2022: 17th European Conference, Tel Aviv, Israel, October 23–27, 2022, Proceedings, Part II*, pages 730–747. Springer, 2022.

Michael M. Bronstein, Joan Bruna, Taco Cohen, and Petar Veličković. Geometric deep learning: Grids, groups, graphs, geodesics, and gauges, 2021.

Zihang Dai, Hanxiao Liu, Quoc V Le, and Mingxing Tan. Coatnet: Marrying convolution and attention for all data sizes. *Advances in Neural Information Processing Systems*, 34:3965–3977, 2021.

Li Yuan, Yunpeng Chen, Tao Wang, Weihao Yu, Yujun Shi, Zi-Hang Jiang, Francis EH Tay, Jiashi Feng, and Shuicheng Yan. Tokens-to-token vit: Training vision transformers from scratch on imagenet. In *Proceedings of the IEEE/CVF International Conference on Computer Vision*, pages 558–567, 2021.

Minghao Chen, Kan Wu, Bolin Ni, Houwen Peng, Bei Liu, Jianlong Fu, Hongyang Chao, and Haibin Ling. Searching the search space of vision transformer. *Advances in Neural Information Processing Systems*, 34:8714–8726, 2021.

Jia Deng, Wei Dong, Richard Socher, Li-Jia Li, Kai Li, and Li Fei-Fei. Imagenet: A large-scale hierarchical image database. In *CVPR*, pages 248–255. Ieee, 2009.

Ilija Radosavovic, Raj Prateek Kosaraju, Ross Girshick, Kaiming He, and Piotr Dollár. Designing network design spaces. In *CVPR*, 2020.

Hugo Touvron, Matthieu Cord, Matthijs Douze, Francisco Massa, Alexandre Sablayrolles, and Hervé Jégou. Training data-efficient image transformers & distillation through attention. In *International Conference on Machine Learning*, pages 10347–10357. PMLR, 2021.

Alex Krizhevsky, Vinod Nair, and Geoffrey Hinton. The cifar-10 dataset. *online*: <http://www.cs.toronto.edu/kriz/cifar.html>, 55(5), 2014.

MMSegmentation Contributors. MMSegmentation: Openmmlab semantic segmentation toolbox and benchmark. <https://github.com/open-mmlab/mms Segmentation>, 2020.

Tete Xiao, Yingcheng Liu, Bolei Zhou, Yuning Jiang, and Jian Sun. Unified perceptual parsing for scene understanding. In *Proceedings of the European conference on computer vision (ECCV)*, pages 418–434, 2018.

Bolei Zhou, Hang Zhao, Xavier Puig, Sanja Fidler, Adela Barriuso, and Antonio Torralba. Scene parsing through ade20k dataset. In *Proceedings of the IEEE conference on computer vision and pattern recognition*, pages 633–641, 2017.

Kunchang Li, Yali Wang, Junhao Zhang, Peng Gao, Guanglu Song, Yu Liu, Hongsheng Li, and Yu Qiao. Uniformer: Unifying convolution and self-attention for visual recognition. *arXiv preprint arXiv:2201.09450*, 2022.

Ze Liu, Yutong Lin, Yue Cao, Han Hu, Yixuan Wei, Zheng Zhang, Stephen Lin, and Baining Guo. Swin transformer: Hierarchical vision transformer using shifted windows. In *Proceedings of the IEEE/CVF International Conference on Computer Vision*, pages 10012–10022, 2021b.

Jianwei Yang, Chunyuan Li, Pengchuan Zhang, Xiyang Dai, Bin Xiao, Lu Yuan, and Jianfeng Gao. Focal self-attention for local-global interactions in vision transformers. *arXiv preprint arXiv:2107.00641*, 2021.

Xiangxiang Chu, Zhi Tian, Yuqing Wang, Bo Zhang, Haibing Ren, Xiaolin Wei, Huaxia Xia, and Chunhua Shen. Twins: Revisiting the design of spatial attention in vision transformers. *Advances in Neural Information Processing Systems*, 34:9355–9366, 2021.

Chen-Yu Lee, Saining Xie, Patrick Gallagher, Zhengyou Zhang, and Zhuowen Tu. Deeply-supervised nets. In *Artificial intelligence and statistics*, pages 562–570. PMLR, 2015.

Giuseppe Peano. Sur une courbe, qui remplit toute une aire plane. *Mathematische Annalen*, 36(1):157–160, 1890.

George F Simmons. *Introduction to topology and modern analysis*, volume 44. Tokyo, 1963.

David Hilbert. Über die stetige abbildung einer linie auf ein flächenstück. In *Dritter Band: Analysis· Grundlagen der Mathematik· Physik Verschiedenes*, pages 1–2. Springer, 1935.

Jian Zhang, Sei-ichiro Kamata, and Yoshifumi Ueshige. A pseudo-hilbert scan algorithm for arbitrarily-sized rectangle region. In *International Workshop on Intelligent Computing in Pattern Analysis and Synthesis*, pages 290–299. Springer, 2006.

Lutz Tautenhahn. Draw a space-filling curve of arbitrary size. http://lutanho.net/pic2html/draw_sfc.html, 2003.

Ross Wightman. Pytorch image models. <https://github.com/rwightman/pytorch-image-models>, 2019.

Donald J Berndt and James Clifford. Using dynamic time warping to find patterns in time series. In *KDD workshop*, volume 10, pages 359–370. Seattle, WA, USA:, 1994.

Meinard Müller. Dynamic time warping. *Information retrieval for music and motion*, pages 69–84, 2007.

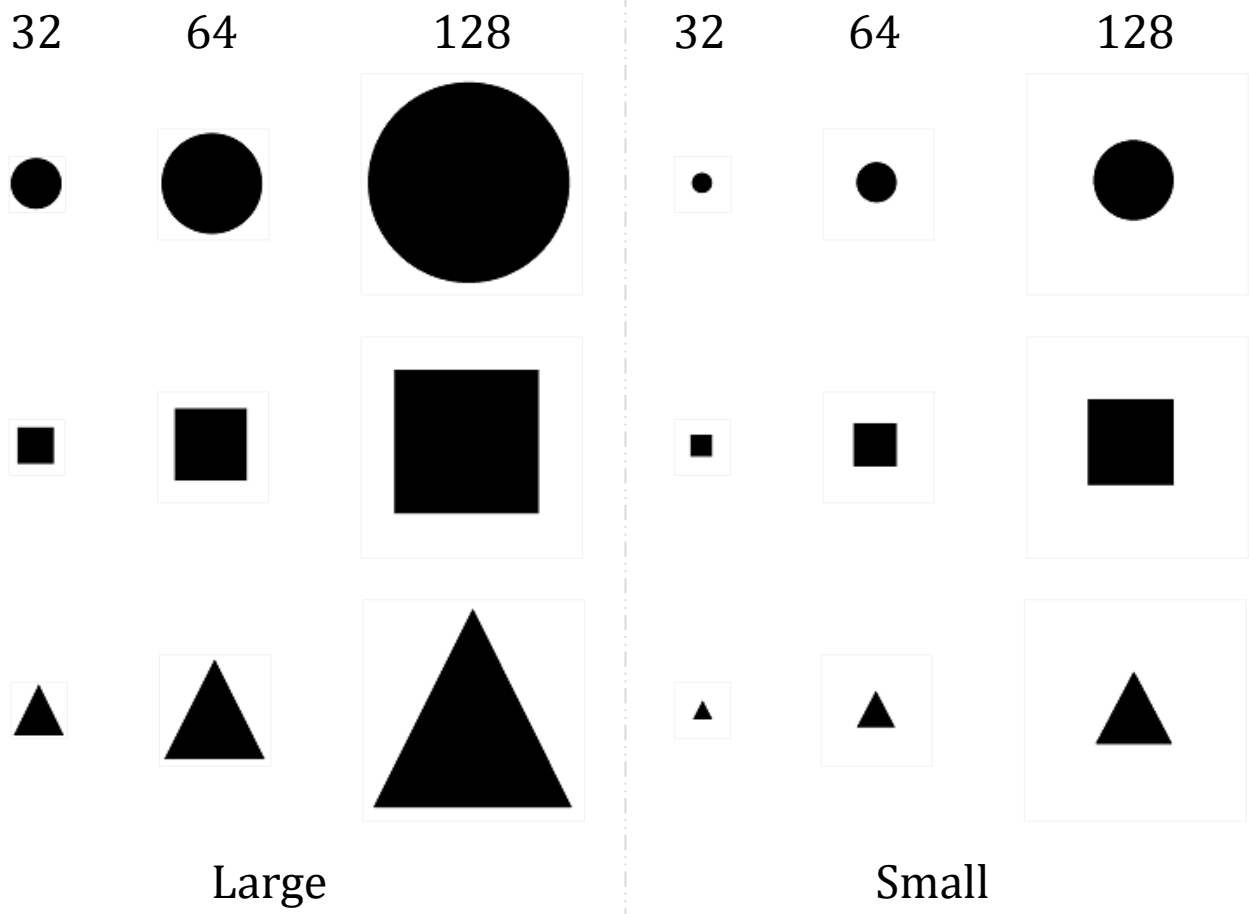


Figure 6: Three common image shapes including “circle”, “square” and “triangle” are generated. Each shape consists of three resolutions (32×32 , 64×64 , 128×128) and two target scales (large and small).

Table 7: The outline of the proposed network architecture FPN-MLPs. The output size of each block is the input size of the next one see Fig. 5 in the main article. From top to bottom, the components appear in sequence. Each component may appear multiple times in FPN-MLPs.

Type	Patch size/Stride or Remarks	Input Size
Conv1D	$7 \times 1/1$	3×1024
Conv1D	$5 \times 1/2$	64×256
Conv1D	$3 \times 1/2$	256×64
Conv1D	$3 \times 1/2$	512×16
Conv1D	$3 \times 1/1$	$3 \times 1024/256/64/16$
Conv1D	$1 \times 1/1$	$3 \times 1024/256/64/16$
GELU	$3 \times 1/1$	$3 \times 1024/256/64/16$
LayerNorm	$3 \times 1/1$	$3 \times 1024/256/64/16$
AvgPool1D	16×1	512×16
Linear	<i>Logits</i>	1×512
Softmax	<i>Classifier</i>	1×10

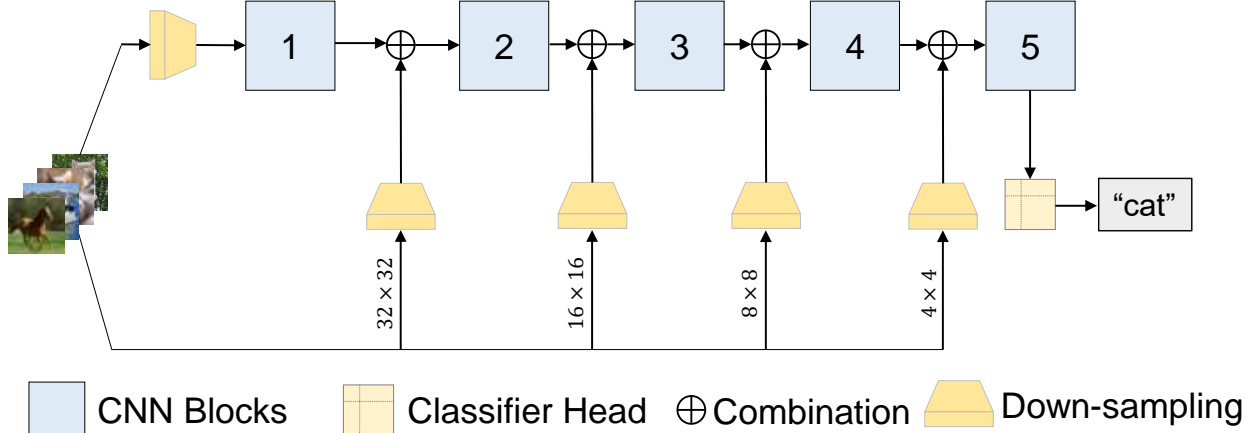


Figure 7: The pipeline of our FPN-MLPs network. The FPN-MLPs consist of the residual branch and a backbone network. The residual branch (below) includes an image down-sampling pyramid structure and MLPs.

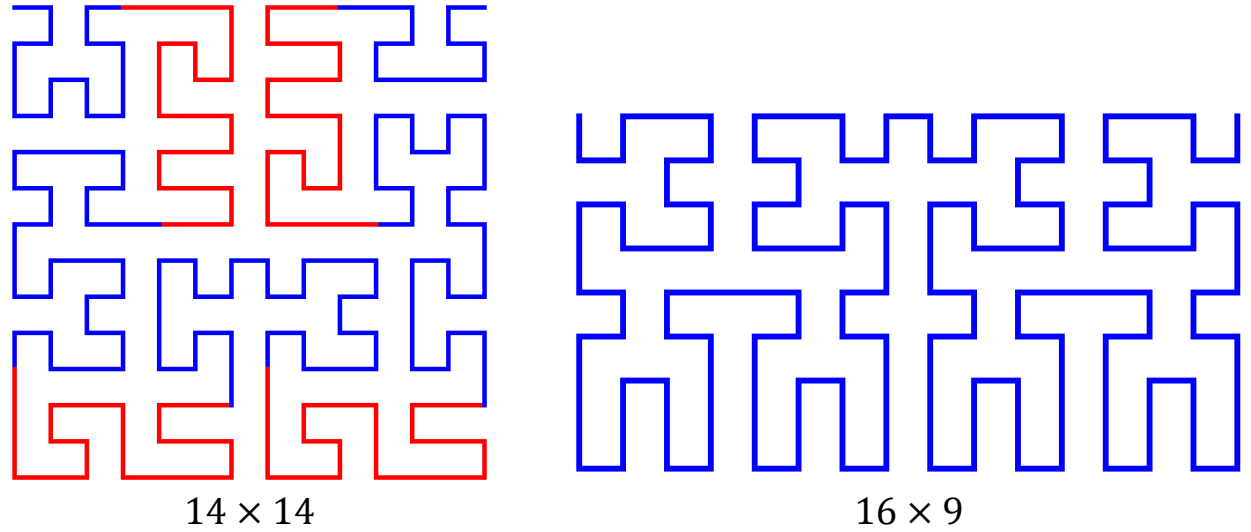


Figure 8: Thanks to Zhang et al. [2006] and Tautenhahn [2003], we show here examples of arbitrary Hilbert flattening. Left: at resolution 14×14 , Right: at resolution 16×9 .

A Preliminaries

A.1 Space-Filling Curves

A continuous curve is called *space-filling curve* if it can pass through every point of a closed square Peano [1890]. More precisely, a space-filling curve is a continuous mapping from a closed unit interval $I = [0, 1]$ to a closed unit square $Q = [0, 1]^2$ Simmons [1963]. It is defined as follows:

Definition 3 A mapping $f: I \rightarrow E^n (n \geq 2)$ is continuous and $f(I)$ has positive Peano–Jordan measure, then $f(I)$ is called a space-filling curve, where E^n denotes an n -dimensional Euclidean space.

Hilbert curve Hilbert [1935] is the first generic geometric program that allows to construct entire classes of space-filling curves. Compared to zigzag curves and Gray-encoded curves, Hilbert curves were the best at minimizing the number of clusters Jagadish [1990].

Table 8: The DTW distance for different target sizes and image resolutions. Lower is better. (“L32” means Large scale image with a resolution of 32×32 and “S32” means Small scale image with a resolution of 32×32 .)

Scale Methods	L32 VS. S32		L32 VS. L64		L64 VS. S64		L64 VS. L128		L128 VS. S128		L32 VS. S128	
	HF	ZF	HF	ZF	HF	ZF	HF	ZF	HF	ZF	HF	ZF
Circle	5.19	8.61	4.13	14.32	6.14	16.28	6.74	28.71	9.13	33.31	3.95	18.52
Square	3.40	8.14	5.42	17.16	6.60	15.53	7.39	35.47	10.58	31.03	8.67	29.67
Triangle	4.61	9.60	3.63	16.03	6.93	18.83	6.06	31.55	7.99	38.07	4.30	10.28

B Experiment Details

The demo dataset for compute the Dynamic Time Warping Distance is shown in Fig. 6.

The outline of the proposed network architecture FPN-MLPs is shown in Table 7 and Fig. 7.

Training. We conducted a large number of image classification experiments on the ImageNet. We also perform the instance segmentation task to analyze the scale robustness of our HPE on ADE20K. We train all backbones from scratch with a fixed input resolution (224×224) on ImageNet. We follow the same settings in DeiT by default, consist of the data augmentation and regularization. Meanwhile, we set drop path rate as 0.1/0.35/0.45 respectively for our HPE with ViT-S/B/L. All models are trained with “AdamW” optimizer with the cosine learning rate schedule for 300 epochs, while the first 10 epochs are applied for linear warm-up. The weight decay, learning rate and batch size are set to 0.05, 1e-3 and 1024 respectively. We experimented with 4 NVIDIA A100 GPUs under the single virtual environment Python 3.7 and Torch 1.7.1.

Fine-tuning. We finetune all ViT backbones on a larger image resolution, i.e., 336×336 and 384×384 for ViT-S/B, respectively. During the finetune phase, the weight decay, learning rate, batch size, warm-up epoch and total epoch are set to 0.1, 1e-5, 256, 10 and 30.

Implementation. An implementation of our HPF and reverse Hilbert flattening are reported below. The detailed training code (our code most base on timm Wightman [2019]) and the model will be made public soon.

```

1  class HilbertPatchFlatten(object):
2      def __init__(self, index):
3          self.inter_index, self.intra_index = index[0], index[1]
4          self.p_s = int(math.sqrt(self.inter_index.shape[0]))
5
6      def __call__(self, img):
7          ra1 = Rearrange(b c (h p1) (w p2) -> b c h w p1 p2, p1=self.p_s,
8                           p2=self.p_s)
8          img = ra1(img)
9          img = img[:, :, self.intra_index[:, 0], self.intra_index[:, 1], :,
10                     :]
10         img = img[:, :, :, self.inter_index[:, 0], self.inter_index[:, 1]]
11         ra2 = Rearrange(b c n H -> b n (H c))
12         img = ra2(img)
13         return img
14
15     def reverse_hilbert_flatten_(x, h, w):
16         index = Gilbert(h, w).index_down
17         b, hw, c = x.shape
18         temp = torch.zeros((b, h, w, c))
19         temp[:, index[:, 0], index[:, 1], :] = x
20         return temp

```

Generalization Capacity of HF. Towards a simplified theoretical analysis, we focus on the grid with equal size of height and width (2^n). As shown in Fig. 8, following a simple recursive algorithm proposed in Tautenhahn [2003], Zhang et al. [2006], the general HF can cover grid with arbitrary size.



Figure 9: Qualitative results of the 1D interpolation-based image scaling. (a) After expanding the image from 2D to 1D with ZF, we downsample the original image to 256×256 by the nearest neighbor 1D interpolation algorithm. (b) Again, we do the dimensional transform with ZF first, upsample the original image to 512×512 by the same algorithm. (c) Same as (a), but with HF. (d) Same as (b), but with HF. (e) 512×512 resolution original ‘‘Lena’’ image. (f) 256×256 resolution original image.

C Additional Analyses

C.1 Image Scaling

Image scaling is a common operation in digital image processing (DIP). Two interpolations by row and column respectively are the standard practice for image scaling. But, if we expand the image and interpolate it only once, will this scale the image properly? As shown in Fig. 9 (a) and (b), with ZF method, neither up-sampling nor down-sampling operations result in a normal image. On the contrary, with HF strategy, see Fig. 9 (c) and (d), the normal results are obtained regardless of the upsampling or downsampling operation. Moreover, the scaling effect of HF can perform favorably against the result of 2D interpolation algorithms.

C.2 Dynamic Time Warping Distance.

Dynamic time warping (DTW) is a prominent approach to obtain an optimal alignment between two given (One-Dimension) sequences under certain restrictions Berndt and Clifford [1994]. Initially, DTW was commonly utilized to compare different speech modalities in automatic speech recognition, see Müller [2007]. Here, we produced a demo dataset consisting of three common shapes (circle, square, and triangle), see details in Appendix. All the images are first flattened into an 1D form by two different unfolding strategies (HF VS. ZF, see Fig. 1), and then the DTW distance between any two images is calculated. The detailed results are reported in Table 8. When the resolution of the two

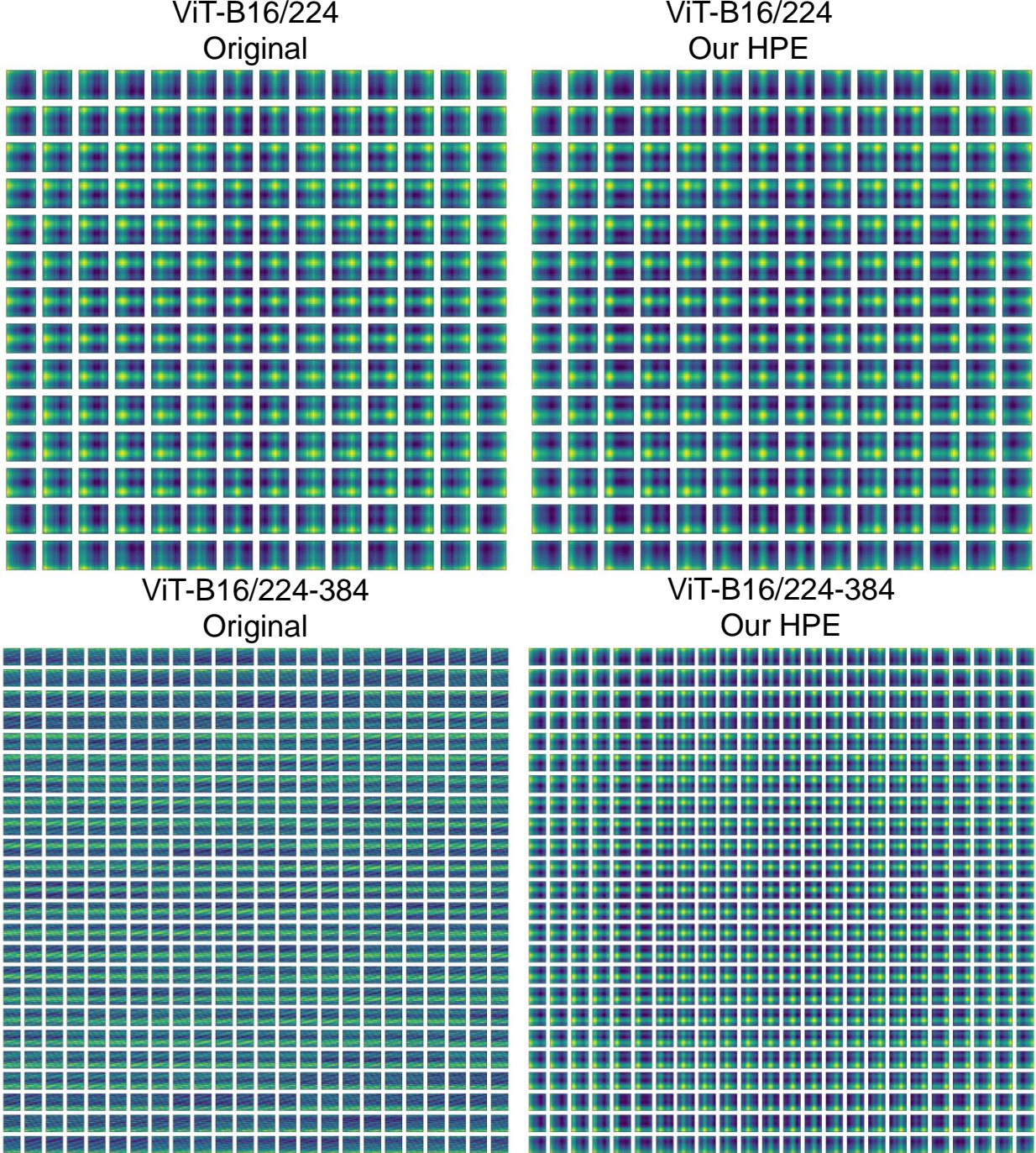


Figure 10: Similarity of position embeddings of ViT-B16 with different patch embedding approaches. The brightness of a pixel indicates the cosine similarity between the position embedding of one patch with the indicated row and column and the other patches. We plot all patches (14×14) for visualization (two figures on the top). The two figures below are obtained by linear interpolation of the original position embedding. Same as the top figures, all patches (24×24) are shown for visualization.

images is equal, turn up the resolution, DTW distance between large and small targets will also follow the increase. However, The change of DTW value in HF is very small compared to ZF. When the target scale of the two images is equal, turn up the resolution of both, the DTW distance between different resolutions will also follow the increase. HF

is still the method with the least variation in DTW values. In addition, the DTW value of HF is always the smallest one among all settings, and at the smallest it is only one-fifth of ZF.

C.3 Details of Position Embeddings

As described in the main paper, here we report specific and detailed similarity of position embeddings, as shown in Fig 10. We can see that, the HPE method has more precise position indication, while the original method is susceptible to horizontal or vertical position points. Additionally, when performing re-scaling on the position encoding matrix, HPE can keep most of the position information, while the original method loses the horizontal position information.

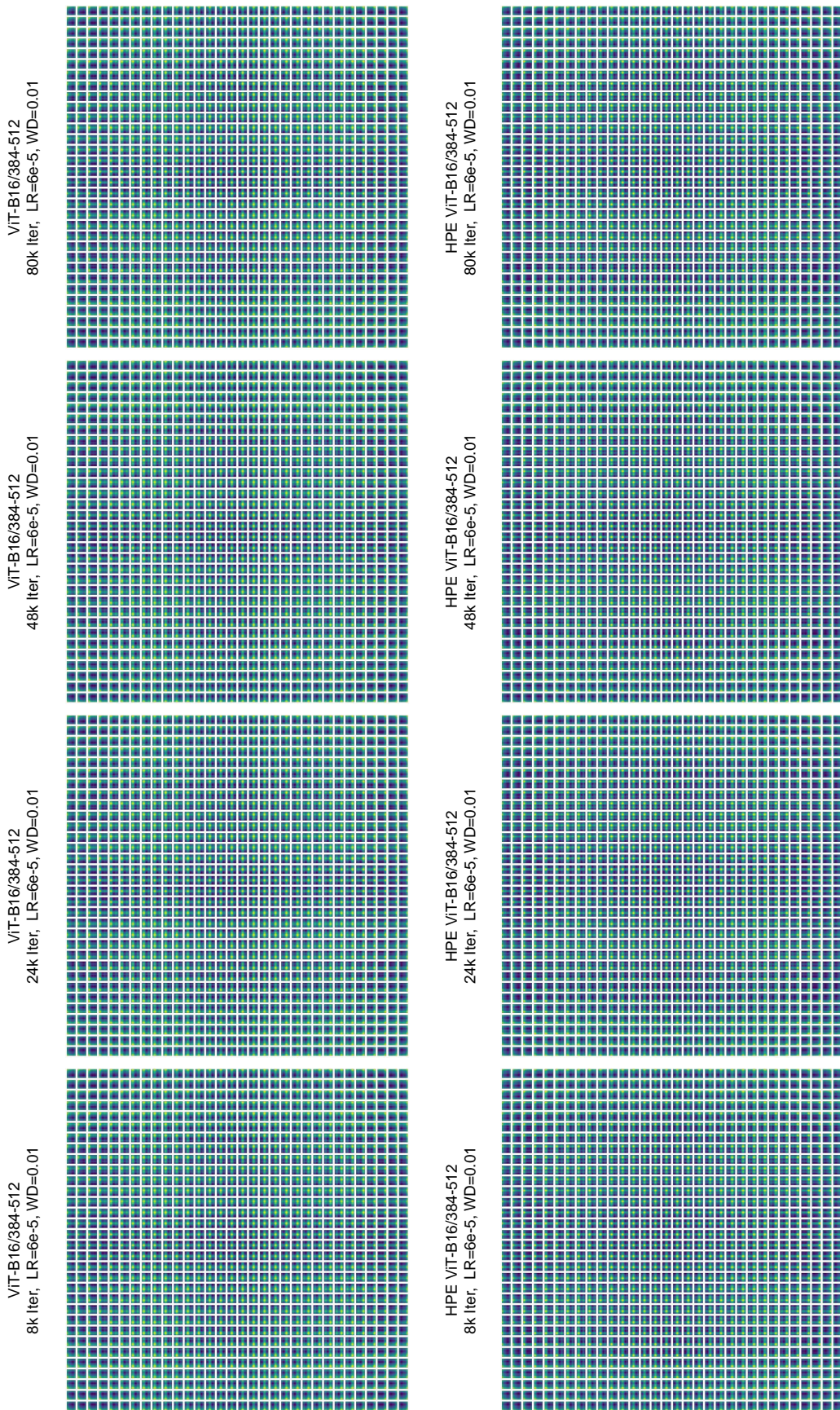


Figure 11: The position embeddings of backbones trained with different patch embedding approaches on ADE20K
 Zhou et al. [2017].